Intermediate regime between metal and superconductor below T=100 K in NiSi

Ashutosh Dahal,[1] Jagath Gunasekera,[1] Leland Harriger,[2] S. H. Lee,[3] Y. S. Hor,[3] David J. Singh,[1] and Deepak K. Singh[1,*]

[1]*Department of Physics and Astronomy, University of Missouri, Columbia, Missouri 65211, USA*

[2]*National Institute of Standards and Technology, Gaithersburg, Maryland 20899, USA*

[3]*Department of Physics, Missouri University of Science and Technology, Rolla, Missouri 65409, USA*

(Received 6 June 2016; revised manuscript received 6 November 2016; published 28 November 2016)

Magnetic response of a metal to an external magnetic field remains independent of the frequency of an ac magnetic field as temperature is reduced. Here, we report the discovery of an anomalous but enormous enhancement of the ac frequency dependent diamagnetic susceptibility below $T \simeq 100$ K in metallic NiSi. In addition, magnetic measurements of NiSi in applied magnetic field depict strong irreversibility in the diamagnetic responses of zero-field cooled and field cooled curves below $T \simeq 55$ K. Even though the metallic behavior of NiSi is primarily manifested to the lowest temperature of $T = 1.5$ K, a small downward cusp around $T \simeq 75$ K is also detected in electrical measurement. These observations suggest the existence of a minority superconducting phase in NiSi, which bridges the gap between metal and superconductor. Consequently, this novel intermediate regime provides a new perspective to the development of unconventional superconductors.

DOI: 10.1103/PhysRevB.94.184516

I. INTRODUCTION

The discovery of superconductivity in iron pnictides and chalcogenides has spurred vigorous studies of nonmetal-based solid state materials [1–4]. The experimental investigations, connecting magnetic ion vacancies to the underlying magnetism and the superconducting state, in alkali-metal intercalated iron selenides provide a new perspective to the current understanding [5]. Silicides, being neighbor to pnictides and chalcogenides, are interesting in their own right. For instance, monosilicides MSi, where M is a magnetic ion with $3d$ electronic configuration (Mn, Fe, Ni, Cr, etc.), provide a rich avenue to study novel magnetism of fundamental importance, such as skyrmion lattice (MnSi), unconventional magnetic insulator (FeSi), and spin singlet state (CoSi) [6–9]. In many cases, however, the noncentrosymmetric cubic structure plays key role. In addition to the novelty in the fundamental properties, some of these materials are also used extensively for technological applications [10]. For instance, NiSi, with FeAs-type orthorhombic crystal structure, is widely used in the microelectronics industry to create contact for the field-effect transistor or the nanoelectronic devices [11,12]. Both electron and hole carriers, deriving from large Fermi surfaces, participate in the electrical conduction in NiSi [13,14]. Despite the enormous technological significance of NiSi metal, its magnetic properties are largely unexplored due to the apparent nonmagnetic ground state [14]. Detailed investigation of the magnetic properties in polycrystalline NiSi using the complementary techniques of ac susceptibility, electrical, neutron scattering, and dc susceptibility measurements reveals unexpected new properties. We show that NiSi exhibits a minority superconducting phase, which coexists with the majority metallic phase below $T < 100$ K.

II. EXPERIMENTS

The polycrystalline samples of NiSi were synthesized by conventional solid state reaction method using ultrapure ingredients of Ni (99.996% purity) and Si (99.999% purity) powders. Starting materials were mixed in stoichiometric composition, pelletized and sintered at 970° for 24 h in a sealed quartz tube, and evacuated to the pressure of 10^{-4} torr. The sample was cooled slowly to room temperature in another 8 h. Samples were characterized using Siemens D500 powder x-ray diffractometer. The shiny sample exhibited pure NiSi phase. The x-ray diffraction (XRD) data was refined using the Rietveld powder diffraction refinement. As shown in Fig. 1, all peaks in the x-ray diffraction pattern fit to the NiSi phase, thus confirming the single phase of the sample. The refined structure was identified with the *Pnma* orthorhombic structure of NiSi, with lattice parameters of $a = 5.186$ Å, $b = 3.331$ Å, and $c = 5.625$ Å, also consistent with other reports on the synthesis of high quality samples of NiSi [13]. The experiment was repeated more than ten times. Very similar results were observed in all experimental attempts. Detailed ac and dc susceptibility measurements were performed using a Quantum Design physical properties measurement system with a temperature range of 2–300 K and a magnetic properties measurement system, respectively. A four-probe technique was employed to measure the electrical resistance of NiSi. For the four-probe measurements, equidistant contacts were made on a 5 mm size sample (as shown in the inset of Fig. 2). Inelastic neutron scattering measurements were performed on 3.1 g pristine powder of NiSi on SPINS cold triple-axis spectrometer at the NIST Center for Neutron Research with a fixed final neutron energy of 5 meV. Neutron scattering measurements employed a cold Be filter followed by a radial collimator and the focused analyzer. The incoherent scattering from vanadium is used to determine the spectrometer's resolution in the specified configuration. At this fixed final energy, the spectrometer's resolution (FWHM) was determined to be $\simeq$0.28 meV.

III. RESULTS

In Figs. 2(a) and 2(b), we plot the ac susceptibility data as a function of temperature for the ac frequency range of 10–10^4 Hz. The magnitude of the ac magnetic field was 10 Oe.

*singhdk@missouri.edu

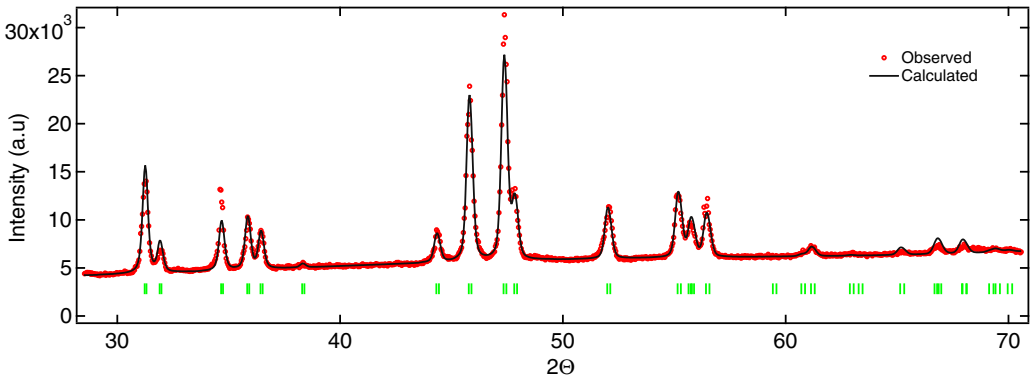

FIG. 1. X-ray diffraction pattern of NiSi. Powder x-ray diffraction spectra of NiSi powder, used in this study. The powder diffraction data is refined using FULLPROF suite for Rietveld analysis. The high purity of the sample is evident from the XRD data, where every single peak is identified to the orthorhombic structure (crystallographic group *Pnma*) of NiSi.

The net ac susceptibility $\chi\ (T)$ is written as $\chi(T) = \chi'(T) + i\chi''(T)$, where the real part ($\chi'$) represents static magnetic behavior and the imaginary part (χ'') provides information about the energy loss due to damping in a system. It is immediately noticed that as the temperature is reduced, both static (χ') and dynamic (χ'') susceptibilities develop highly unusual frequency dependencies below $T \simeq 100$ K. While χ' becomes more negative and tends to saturate at low temperature, χ''

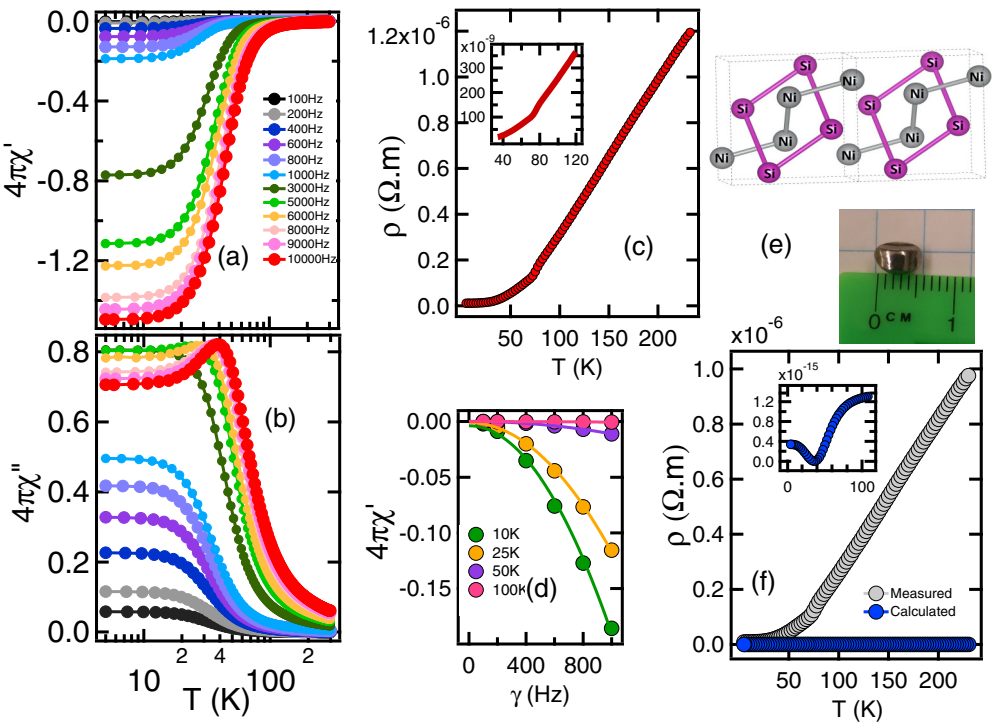

FIG. 2. Frequency dependence of diamagnetism in NiSi. (a) and (b) The ac susceptibility measurement as a function of temperature of NiSi. The ac frequency varies from 10 to 10^4 Hz. NiSi exhibits diamagnetic behavior throughout the measurement temperature range. In a remarkable observation, the static susceptibility χ' is found to develop frequency dependence below $T \simeq 100$ K. The diamagnetic response becomes stronger as ac frequency increases. For the same measurement range of temperature and frequency, bulk dynamic susceptibility χ'' exhibits a peak-type positive response. The peak-type feature moves to higher temperature and becomes stronger as the ac frequency increases. A superconductor usually exhibits these behaviors. However, NiSi is a metal, as depicted by the measurement of electrical resistance as a function of temperature in (c). (c) Very low electrical resistivity, consistent with previous reports on a high quality sample of NiSi, is detected across the entire measurement range of electrical resistivity. The inset highlights a small sharp drop in resistivity at $T \simeq 75$ K. (d) χ' as a function of frequency at a few characteristic temperatures are shown in this figure. The static susceptibility data is extrapolated to obtain the susceptibility value in zero frequency or dc limit $\chi_0(T)$, using the formula $\chi(T) = \chi_0(T) + \alpha(T)\nu^2$, where α is the temperature-dependent quantity. (e) NiSi crystallizes in the orthorhombic structure. The schematic also shows the isotropic nature of the nearest-neighbor exchange interaction. (f) Electrical resistance due to the normal skin effect, as derived from the static susceptibility at $\nu = 10$ KHz, is plotted with experimental resistance data in light gray. Clearly, the experimental data is not described by the normal skin effect, thus ruling out this possibility.

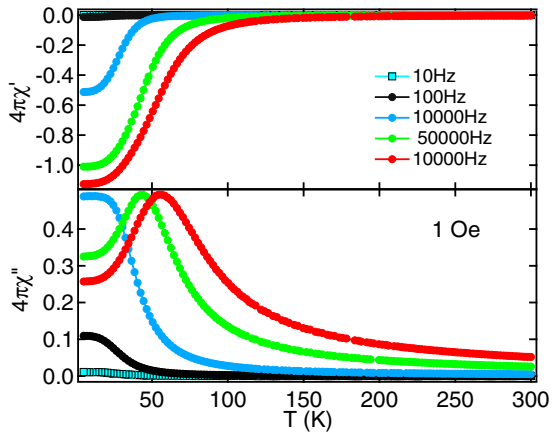

FIG. 3. ac susceptibility measurements in 1 Oe field. The ac susceptibility measurements were also performed in a smaller ac excitation field. Here we plot both the static and the dynamic susceptibilities as a function of temperature at different ac frequencies. The ac excitation field was $H_{ac} = 1$ Oe. The broad features in χ'' at $H_{ac} = 10$ Oe [Fig. 2(b)] become sharp peak-type features at lower ac field. Also, the strong diamagnetism in χ' in NiSi is still observable. Only a superconductor exhibits these properties.

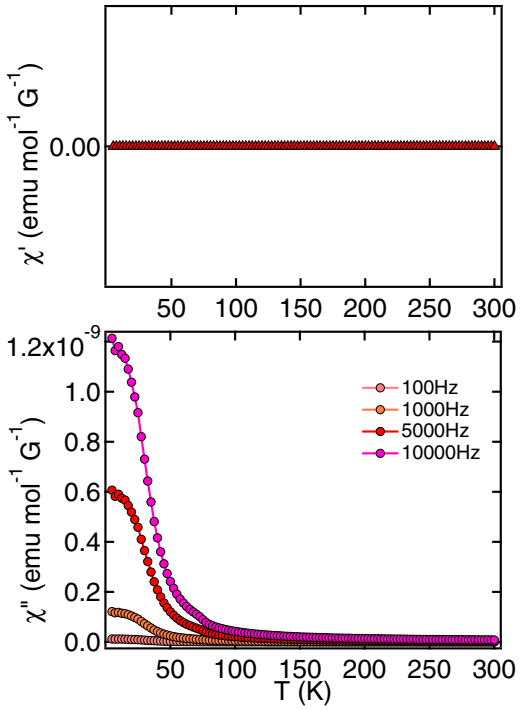

FIG. 4. Plots of χ' and χ'' as deduced from the electrical resistance of NiSi. The calculated ac susceptibilities for a few different ac frequencies using the intergranular interaction between the penetrating flux in different grains. Clearly, it does not explain the experimental data.

becomes more positive and tends to form a peak-type structure at low temperature. This is more evident in Fig. 3, where the measurements of ac susceptibilities in 1 Oe ac magnetic field exhibiting sharp peaks in χ'' are observed. Such frequency dependence of ac susceptibility is the hallmark of a superconductor [15,16]. A small but clearly noticeable feature in the electrical resistivity plot, Fig. 2(c), involves a sharp downward turn at $T \simeq 75$ K, which is similar to the onset temperature of diamagnetism in Fig. 2(a). The frequency dependence of the diamagnetic response in χ' becomes conspicuous below the characteristic temperature $T \simeq 100$ K [Fig. 2(d)]. At $T \geqslant 100$ K, NiSi exhibits temperature and ac frequency-independent diamagnetic character and thus behaves as a good metal.

First we consider the most common mechanism, the normal skin effect in a metal, which can shed light on the anomalous frequency and temperature dependencies of susceptibilities in NiSi. The effect is most pronounced when the skin depth, δ, is maximum, or, when $\delta \simeq R$ for a finite sample of size R [17]. It results in maximum damping loss, hence the χ'' becomes maximum. The corresponding χ', given by $4\pi\chi' = (\delta/2R)\tanh(2R/\delta) - 1$, at the maximum skin depth becomes negligible. This is opposite to our observations in Figs. 2(a) and 2(b). In NiSi, both quantities χ' and χ'' maximize at the same frequency. Also, the skin effect resistance, derived from χ', does not match the experimental data at all [Fig. 2(f)]. An alternative scenario involves the intergranular interaction between penetrating field flux. Although this behavior is much more pronounced in a polycrystalline high temperature superconductor, it can also be applicable in a metal as long as the ac measurement frequency is very low and the penetrating flux in different grains of the sample behave as if the thermally activated vortex jumps between favorable metastable states of the vortex lattice (in a high temperature superconductor). The electrodynamics of a high-T_c superconductor is same as the electrodynamics of a normal metal in thermally activated flux flow regime, i.e., where the Ohm's law is still valid. Such a scenario leads to a distinct loss in χ'' as well as an enhancement in the diamagnetic χ'. Under this formulation, the quantities χ' and χ'' are given by [18]

$$\chi' = \left(\frac{\omega}{\pi\mu_0 H}\int_0^{2\pi/\omega}\langle B\rangle\cos(\omega t)dt\right) - 1, \quad (1)$$

$$\chi' = \left(\frac{\omega}{\pi\mu_0 H}\int_0^{2\pi/\omega}\langle B\rangle\sin(\omega t)dt\right). \quad (2)$$

The calculated plots of χ' and χ'', using the experimental electrical resistance of NiSi, are shown in Fig. 4. While the dynamic susceptibility χ'' is found to increase with the applied ac frequency, the static susceptibility remains negligible. This is very different from the experimental observations. We have also performed the heat capacity measurement in zero field (see Fig. 5). Metallic behavior dominates the heat capacity data, which is not surprising as this is a bulk probe and superconductivity only exists in a very small minority phase in NiSi.

The frequency and temperature dependencies of the diamagnetic response in metallic NiSi are perplexing. To gain insight into this anomalous observation, detailed neutron scattering measurements were performed. The elastic measurement, which is used to detect any magnetic order in a material, show neither additional peaks beyond lattice peaks nor any temperature-dependent enhancement in the lattice peaks at low temperature (Fig. 6). Together, it rules out

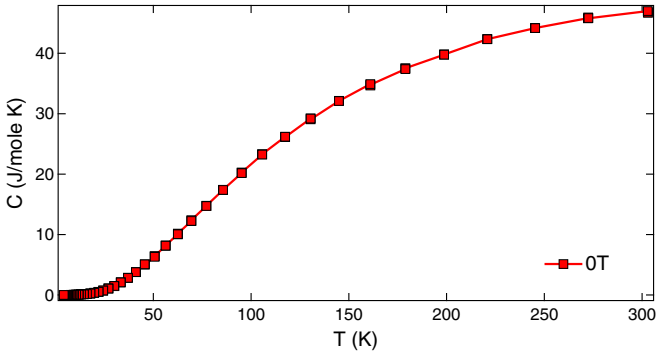

FIG. 5. Heat capacity of NiSi as a function of temperature is shown in this figure. Heat capacity measurement was performed using a Quantum Design physical properties measurement system.

the possibility of any magnetic order, antiferromagnetic or ferromagnetic, in NiSi. Unlike elastic measurements, a broad but well-defined peak centered at $E = 1.75$ meV appears at low temperature in the background corrected inelastic neutron data. Inelastic neutron scattering measurements were performed on a 3.1 g pristine powder of NiSi on SPINS cold triple-axis spectrometer at the NIST Center for Neutron Research with a fixed final neutron energy of 5 meV, at which the spectrometer's resolution (FWHM) was determined to be $\simeq$0.28 meV. $\chi''(Q,E)$ is derived from inelastic neutron data, shown in Fig. 7, using the following relation:

$$S(Q,\omega) = \gamma_0{}^2\left(\frac{k_i}{k_f}\right) f(Q)^2 \frac{1}{1-e^{-\hbar\omega/k_BT}}\left(\frac{\chi''(Q,\omega)}{\pi}\right), \tag{3}$$

where $\gamma_0^2 = 0.073/\mu_B^2$, k_i and k_f represent initial and final neutron wave vectors, and $f(Q)$ is the form factor of magnetic ions (in this case Ni ion). Inelastic data were normalized by

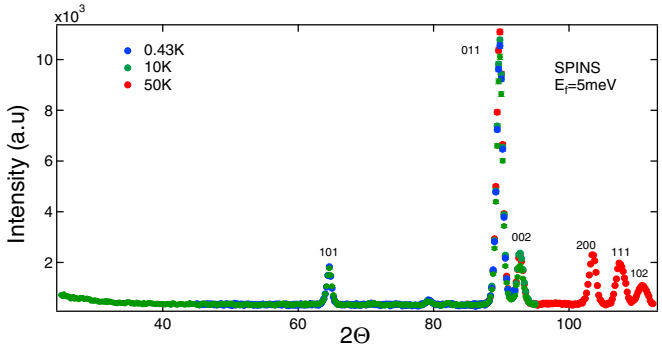

FIG. 6. Elastic neutron scattering measurements on different compositions. High-resolution elastic neutron scattering measurements on powder NiSi were performed on the SPINS cold triple axis spectrometer at the NIST Center for Neutron Research. Observed sharp peaks in this figure are attributed to the nuclear structure factor. No additional peak, indicating antiferromagnetic order, is observed. Also, the difference between the elastic scans data at low temperature and high temperature is found to be statistically insignificant. Together, it rules out the presence of any magnetic order in NiSi. The error bar represents one standard deviation in the experimental data.

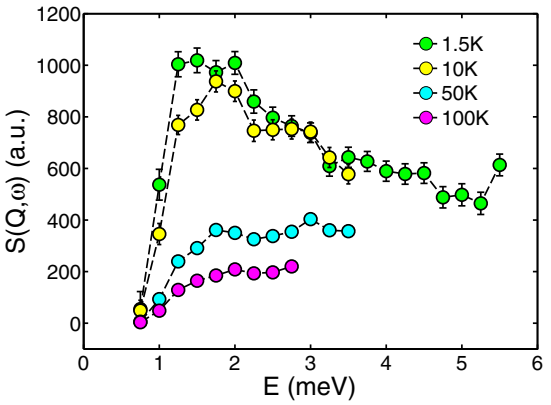

FIG. 7. Inlelastic neutron scattering measurements on NiSi at different temperatures. Thermally balanced inelastic spectra at a fixed $Q = 1.03$ Å at different temperatures are shown in this figure. For this purpose, the background corrected raw data is divided by the factor $[1-\exp(-E/k_BT)]^{-1}$. Inelastic measurements indicate the development of a gapped excitation centered at $E \simeq 1.75$ meV. The error bar represents one standard deviation in the experimental data.

utilizing the incoherent scattering from a vanadium sample of known mass (also used to estimate the resolution of the instrument). Following the normalization procedure by Xu *et al.* [19], we write the normalized dynamic susceptibility as

$$\chi'' = \frac{\pi}{2}\mu_B^2(1-e^{-\hbar\omega/k_BT})S(Q,\omega), \tag{4}$$

where $S(Q,\omega)$ can be written as

$$S(Q,\omega) = \frac{13.77(\text{barns}^{-1})\mu_B^2 I(Q,E)}{|F(Q)^2|e^{-2W}k_iR_0}. \tag{5}$$

The energy integrated incoherent scattering intensity

$$\int I(Q,E)dE = \frac{N}{4\pi}\sum_j \sigma_j^{inc}e^{-2W}k_iR_0 \tag{6}$$

was obtained by performing a $\Delta E = 0$ scan at a wave vector Q. Therefore, we have

$$Nk_iR_0 = 4\pi\frac{\int I(Q,E)dE}{\sum_j \sigma_j^{inc}e^{-2W}}. \tag{7}$$

The variation of the Debye-Waller factor ($e^{-2W} \simeq 1$) was neglected in the calculation. The standard vanadium sample (with a net mass of 0.0373 mol) is used to estimate the total number of unit cells (N) in $N_{\text{vanadium}}k_fR_0$. The incoherent inelastic scan on the vanadium sample was performed under the same instrument configuration as used in experiments on NiSi. The normalized data at $T = 1.5$ K is plotted in Fig. 8.

In Fig. 9, we plot the dynamic susceptibility, $\chi''(Q,E)$ as a function of neutron energy transfer $E = E_i - E_f$ at different temperatures at a fixed wave vector $Q = 1.03$ Å^{-1}. An inelastic peak in the dynamic susceptibility in Fig. 9, centered at $E \simeq 1.75$ meV, at the fixed wave vector $Q = 1.03$ Å is clearly observed as a function of energy. As the measurement temperature increases, the peak intensity decreases. The temperature dependence of the dynamic susceptibility suggests magnetic nature of the dynamic properties.

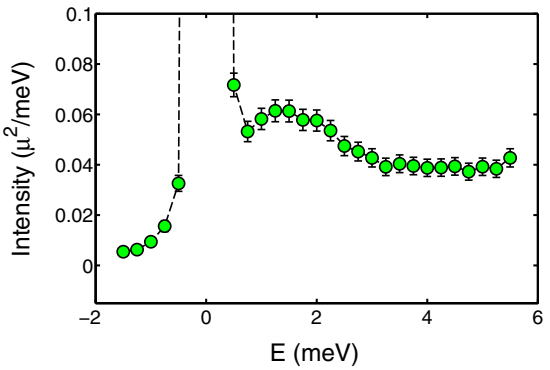

FIG. 8. Full inelastic neutron scattering measurement data at $T = 1.5$ K. Full inelastic scan at $Q = 1.03$ Å^{-1} at $T = 1.5$ K on NiSi is plotted here. The experimental data is background corrected, thermally balanced, and normalized with respect to the vanadium scattering of known mass.

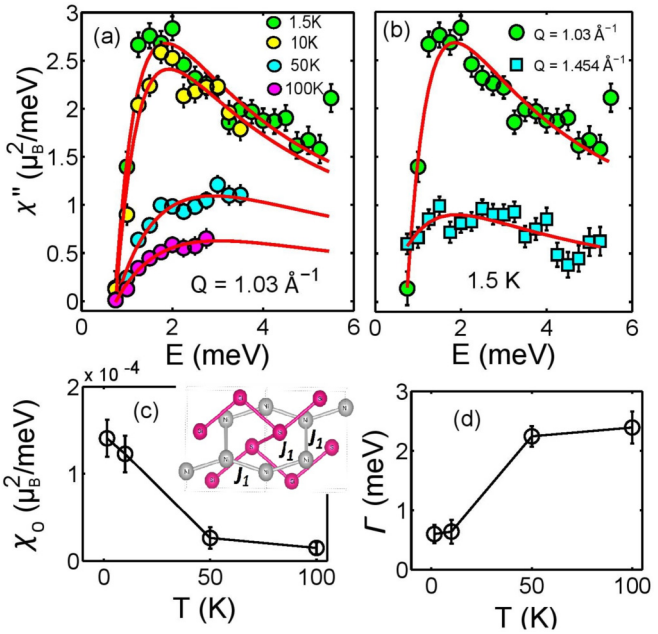

FIG. 9. Dynamic susceptibility, $\chi''(Q,E)$, as a function of energy of NiSi. (a) $\chi''(Q,E)$ is deduced from inelastic neutron scattering data as a function of energy transfer, $E = E_i - E_f$. Inelastic data were background corrected and normalized with respect to the incoherent scattering from a vanadium sample of known mass. The error bar represents one standard deviation in the experimental data. $\chi''(Q,E)$ vs E at a few different temperatures at $Q = 1.03$ Å^{-1} are shown in this plot. Experimental data are well described by RPA analysis (see text for details). The peak in $\chi''(Q,E)$ is centered at $E = 1.75$ meV and is temperature dependent. (b) $\chi''(Q,E)$ vs E at two different wave vectors of $Q = 1.03$ and 1.45 Å^{-1} at $T = 1.5$ K are shown in this figure. The peak intensity follows the Ni form factor. Along with the temperature dependence in Fig. 9(a), it indicates magnetic nature of the excitation. The peak in χ'' is centered at the same energy at both wave vectors. The inset shows the isotropic nature of the nearest-neighbor exchange interaction. (c) and (d) Obtained values of fitting parameters χ_0 and Γ (full width at half maximum) are plotted as a function of temperature. χ_0 decreases as the measurement temperature increases and becomes very small at $T \simeq 100$ K.

NiSi exhibits strong magnetic dynamic behavior despite the lack of any magnetic order. Such behavior is usually found in quantum magnets, for instance a quantum spin liquid of a spin-1/2 system, or an unconventional superconductor of magnetic origin [20–22]. In the latter case, an inelastic peak depicts a gapped magnetic resonance that exhibits a one-to-one correspondence with the superconducting order parameter [22]. Further quantitative information is obtained by analyzing the wave-vector-dependent $\chi''(Q,E)$ data. An inelastic peak in $\chi''(Q,E)$ is fitted using a random phase approximation (RPA) model [23]. Previously, the RPA model has been successful in describing inelastic phenomena in Ni-based systems [24,25]. Also, it is more accurate in describing the low temperature behavior. As described in Ref. [19], we make two assumptions here: the only appreciable interaction is a nearest-neighbor interaction between Ni ions, J_1, and second, the interaction is isotropic in nature [see Fig. 2(e)]. Under these approximations, $\chi''(Q,E)$ is given by

$$\chi''(Q,\omega) = \sum_{\pm} \frac{\omega \chi_0 \Gamma_{Q^{\pm}}}{{\Gamma_{Q^{\pm}}}^2 + \omega^2} \tag{8}$$

where $\Gamma_{Q^{\pm}} = \Gamma[1 \mp \chi_0 J_1]$. While an RPA model may not be the best possible formulation to describe the dynamic properties of NiSi, this simple relation, consisting of three fitting parameters of Γ, J_1, and χ_0, clearly fits the inelastic peak in $\chi''(Q,E)$ very well. The fitted value of $J_1 = 0.93$ meV/μ_B^2 at $T = 1.5$ K indicates a modest exchange interaction between Ni ions. Obtained values of Γ and χ_0 are plotted as a function of temperature in Figs. 9(c) and 9(d), respectively. The dynamic correlation of Ni-Ni ions, as inferred from χ_0, decreases significantly as $T \to 100$ K. At the same time, the parameter Γ, representing the full width at half maximum of dynamic correlation or the inverse of relaxation time τ, increases as a function of temperature. Therefore, magnetic fluctuation has a shorter relaxation time at higher temperature. The magnetic nature of $\chi''(Q,E)$ is further verified from inelastic measurement at higher wave vector $Q = 1.45$ Å^{-1}. A significant reduction in the peak intensity [see Fig. 9(b)], arising due to the Ni form factor dependence on Q, further confirms the magnetic nature of the excitation.

The analysis of Q-dependent dynamic susceptibility suggests strong spin fluctuation, manifested by the excitation centered at $E = 1.75$ meV. It coexists in temperature with the frequency-dependent ac susceptibilities, with a characteristic temperature of $T \simeq 100$ K. Since ac susceptibilities, both χ' and χ'', are more pronounced at higher frequencies, a possible role of the spin fluctuations in the frequency-dependent diamagnetic response of NiSi cannot be ruled out. However, the energy of correlated spin fluctuation is much smaller compared to the characteristic temperature of the diamagnetic susceptibilities (equivalent to 9 meV or 2.2 THz). Therefore, the spin fluctuation alone may not be the underlying mechanism behind the anomalous diamagnetism in NiSi. Also, there are numerous metallic magnetic materials that exhibit strong spin fluctuation, yet no frequency-dependent diamagnetic response is detected in the bulk susceptibility.

Finally, the dc susceptibility data of NiSi is presented. As shown in Fig. 10, the diamagnetic nature of NiSi is confirmed using the bulk magnetization measurement. The

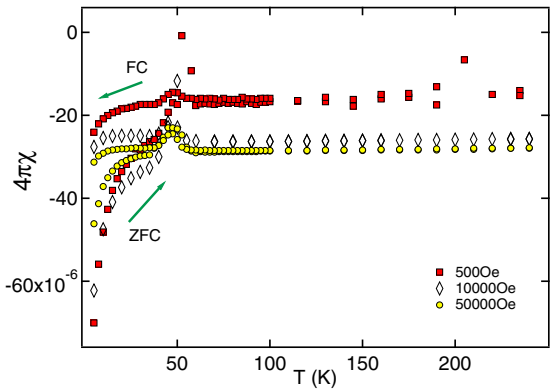

FIG. 10. dc susceptibility measurements of NiSi. Characteristic plots of dc susceptibility as a function of temperature at a few different applied magnetic field values. The diamagnetic nature of nickel silicide is confirmed using dc susceptibility measurements. In addition to that, two distinct features are observed in dc susceptibility data that are generally observed in a superconductor: strong enhancement in the diamagnetic values of ZFC (zero field cooled) and FC (field cooled) below $T \simeq 55$ K, and irreversibility in the ZFC and FC responses to field application. It is also noticed that as the applied field strength increases, the irreversibility becomes weaker.

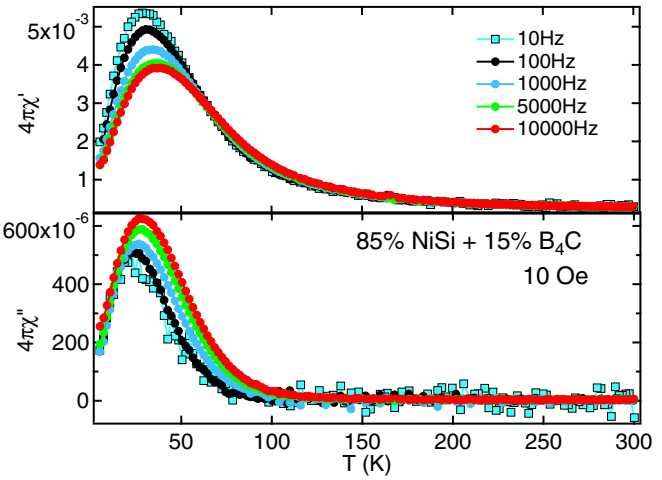

FIG. 11. ac susceptibility measurements of NiSi mixed with mB_4C_3 powder. The ac excitation field was $H_{ac} = 10$ Oe. NiSi powder was mixed with a small amount ($\simeq$15%) of insulating and nonmagnetic mB_4C_3 powder to test the presence of skin effect. As shown here, the diamagnetism completely disappears (a) even though the sample was highly conducting, thus ruleing out skin effect in the system.

bulk susceptibility is found to be similar to the extrapolated value of the static susceptibility (χ') in zero frequency limit, Fig. 2(d). In addition to the diamagnetic behavior, a peak-type feature at $T \simeq 55$ K (discussed below) is observed in dc susceptibility. The peak is followed by the strong enhancement in the diamagnetic signal in both the field cooled (FC) and the zero field cooled (ZFC) curves. FC and ZFC curves exhibit different responses to the diamagnetic enhancement and are thus highly irreversible. Moreover, the strength of the diamagnetic signal becomes weaker as the applied field is increased. In general, a superconducting system exhibits a similar diamagnetic response to magnetic field application [26]. However, the susceptibility of NiSi at $T = 5$ K (1×10^{-4} SI unit) is much smaller compared to the perfect diamagnetic response of a superconductor, i.e., $4\pi\chi = -1$ [27].

IV. DISCUSSION

The anomalous observations in NiSi metal has no precedent in the available literature. The magnetic response of a metal to an external magnetic field is termed as paramagnetic or diamagnetic, depending on the parallel or antiparallel alignment of electron's moment to the applied field, respectively [28–30]. The quantum-mechanical treatment of the metal's bulk properties forbids any frequency or temperature dependence of the diamagnetic response in an ac magnetic field [28,31]. It can be argued that the underlying Fermi surface in NiSi evolves as a function of temperature in applied field. This can cause a temperature-dependent diamagnetism. However, such reconstruction requires a large magnetic field [32]. We note that both anomalies are produced at very small magnetic fields (a few Oe to a few hundred Oe), not sufficient to induce the evolution of the Fermi surface as observed in the de Haas–van Alphen effect measurements. Moreover, the ac frequency dependence of the bulk susceptibility and the irreversibility in the ZFC and FC responses in NiSi sets it apart from a high magnetic field induced behavior in a metallic magnet. Another effect that can cause diamagnetism in a metal is the skin effect. As discussed in the beginning, the analytical calculation clearly rules out the role of skin effect in the diamagnetic properties of NiSi. Measurements were also performed on NiSi, mixed with nonmagnetic insulator boron carbide, to further test the presence of normal skin effect. For this purpose, NiSi powder was mixed with a small amount, 15%, of insulating and nonmagnetic mB_4C_3 powder and measured both the ac susceptibility and the electrical resistance. While the sample was still highly conducting, the diamagnetism completely disappears (see Fig. 11). If it was indeed the normal skin effect, the frequency-dependent response should have persisted, as the high conductivity due to the flow of current in the skin of the material is still preserved. These results further rule out the normal skin effect in the system.

The minority superconducting phase, coexisting with the majority metallic phase in NiSi, is apparent from detailed experimental observations. For instance, electrical measurements on NiSi depict a small downward cusp at $T \simeq 75$ K in otherwise metallic characteristic as a function of temperature. This temperature is similar to the onset temperature of simultaneous maximization of the diamagnetic static susceptibility and the peak-type feature in the dynamic susceptibility in the ac susceptibility measurement, suggesting the presence of a superconducting phase in the system. Also, NiSi exhibits significant diamagnetic response in dc susceptibility measurements below $T \simeq 55$ K. It is also found that the irreversibility between ZFC and FC curves is much stronger at low field, compared to high field. However, the net susceptibility at low temperature ($4\pi\chi \simeq 10^{-4}$) is much less than that of a perfect superconductor ($4\pi\chi = -1$), indicating the minority character of the superconducting phase. We note that the diamagnetic irreversibility between ZFC and FC curves follows a peak-type feature at $T \simeq 55$ K. While its origin is not yet understood, it may be arising due to the

competing effects between the weak paramagnetic nature of the bulk and the minority-superconducting phase that does not percolate to bulk. These arguments infer that NiSi apparently represents a new intermediate regime between a metal and a superconductor, which shares its traits with both states. Further theoretical and experimental works can reveal a closer perspective to the underlying mechanism, which will help in understanding the interesting but puzzling properties of unconventional superconductors.

ACKNOWLEDGMENTS

We thank W. Montfrooij for helpful discussion and experimental assistance. This work used facilities supported in part by the Department of Commerce. D.K.S. gratefully acknowledges support from the U.S. Department of Energy, Office of Basic Energy Sciences under Grant No. DE-SC0014461. Y.S.H. acknowledges support from the National Science Foundation under Grant No. DMR-1255607.

[1] Y. Kamihara, H. Hiramatsu, M. Hirano, R. Kawamura, H. Yanagi, T. Kamiya, and H. Hosono, Iron-based layered superconductor: LaOFeP, J. Am. Chem. Soc. **128**, 10012 (2006).

[2] F.-C. Hsu, J. Luo, K. Yeh, T. Chen, T. Huang, P. Wu, Y. Lee, Y. Huang, Y. Chu, D. Yan, and M. Wu, Superconductivity in the PbO-type structure a-FeSe, Proc. Natl. Acad. Sci. USA **105**, 14262 (2008).

[3] J. M. Tomczak, K. Haule, and G. Kotliar, Signatures of electronic correlations in iron silicide, Proc. Natl. Acad. Sci. USA **109**, 3243 (2012)

[4] A. D. Christianson, E. Goremychkin, R. Osborn, S. Rosenkranz, M. Lumsden, C. Malliakas, I. Todorov, H. Claus, D. Chung, M. Kanatzidis, R. Bewley, and T. Guidi, Unconventional superconductivity in $Ba_{0.6}K_{0.4}Fe_2As_2$ from inelastic neutron scattering, Nature (London) **456**, 930 (2008).

[5] A. Krzton-Maziopa, V. Svitlyk, E. Pomjakushina, R. Puzniak and K. Conder, Superconductivity in alkali metal intercalated iron selenides, J. Phys.: Condens. Matter **28**, 293002 (2016).

[6] U. K. Robler, A. N. Bogdanov, and C. Pfleiderer, Spontaneous skyrmion ground states in magnetic metals, Nature (London) **442**, 797 (2006).

[7] S. Krannich, Y. Sidis, D. Lamago, R. Heid, J.-M. Mignot, H. V. Löhneysen, A. Ivanov, P. Steffens, T. Keller, L. Wang, E. Goering, and F. Weber, Magnetic moments induce strong phonon renormalization in FeSi, Nat. Commun. **6**, 8961 (2015).

[8] N. Manyala, Y. Sidis, J. DiTusa, G. Aeppli, D. Young, and Z. Fisk, Large anomalous Hall effect in a silicon-based magnetic semiconductor, Nat. Mater. **3**, 255 (2004).

[9] O. Delaire, K. Marty, M. Stone, P. Kent, M. Lucas, D. Abernathy, D. Mandrus, and B. Sales, Phonon softening and metallization of a narrow-gap semiconductor by thermal disorder, Proc. Natl. Acad. Sci. USA **108**, 4725 (2011)

[10] L. Chen, Metal silicides: An integral part of microelectronics, JOM **57**, 24 (2005).

[11] H. Iwai, T. Ohguro, and S. Ohmi, NiSi salicide technology for scaled CMOS, Microelectron. Eng. **60**, 157 (2002).

[12] T. Morimoto, T. Ohguro, S. Momose, T. Iinuma, I. Kunishima, K. Suguro, I. Katakabe, H. Nakajima, M. Tsuchiaki, and M. Ono *et al.*, Self-aligned nickel-mono-silicide technology for high-speed deep submicrometer logic CMOS ULSI, Electron. Dev. **42**, 915 (1995).

[13] B. Meyer, U. Gottlieb, O. Laborde, H. Yang, J. Lasjaunia, A. Sulpice, and R. Madar, Intrinsic properties of NiSi, J. Alloys Compd. **262-263**, 235 (1997).

[14] A. Franciosi, J. H. Weaver, and F. A. Schmidt, Electronic structure of nickel silicides Ni 2 Si, NiSi, and NiSi, Phys. Rev. B **26**, 546 (1982).

[15] F. Gomory, Characterization of high-temperature superconductors by AC susceptibility measurements, Supercond. Sci. Technol. **10**, 523 (1997).

[16] R. Singh, R. Lal, U. C. Upreti, D. K. Suri, A. V. Narlikar, V. P. S. Awana, J. Albino Aguiar, and M. Shahabuddin, Superconductivity in Zn-doped tetragonal $LaBaCaCu_3O_7 - \delta$ systems, Phys. Rev. B **55**, 1216 (1997).

[17] M. D. Vannette, Dynamic magnetic susceptibility of systems with long-range magnetic order, Ph.D. thesis, Iowa State University, 2009.

[18] V. B. Geshkenbein, V. M. Vinokur, and R. Fehrenbacher, ac absorption in the high-T_c ac absorption in the high-T c superconductors: Reinterpretation of the irreversibility line superconductors: Reinterpretation of the irreversibility line, Phys. Rev. B **43**, 3748(R) (1991).

[19] G. Xu, Z. Xu, and J. M. Tranquada, Absolute cross-section normalization of magnetic neutron scattering data, Rev. Sci. Instrum. **84**, 083906 (2013).

[20] S.-H. Lee, H. Kikuchi, Y. Qiu, B. Lake, Q. Huang, K. Habicht, and K. Kiefer, Quantum-spin-liquid states in the two-dimensional kagome antiferromagnets $Zn_xCu_{4-x}(OD)_6Cl_2$, Nat. Mater. **6**, 853 (2007).

[21] B. Lake, G. Aeppli, T. Mason, A. Schröder, D. McMorrow, K. Lefmann, M. Isshiki, M. Nohara, H. Takagi, and S. Hayden, Spin gap and magnetic coherence in a clean high-temperature superconductor, Nature (London) **400**, 43 (1999).

[22] J. Tranquada, H. Woo, T. G. Perring, H. Goka, G. D. Gu, G. Xu, M. Fujita, and K. Yamada, Quantum magnetic excitations from stripes in copper oxide superconductors, Nature (London) **429**, 534 (2004).

[23] C. Broholm, J. K. Kjems, G. Aeppli, Z. Fisk, J. L. Smith, S. M. Shapiro, G. Shirane, and H. R. Ott, Spin Fluctuations in the Antiferromagnetic Heavy-Fermion System U_2Zn_{17}, Phys. Rev. Lett. **58**, 917 (1987).

[24] J. F. Cooke, J. W. Lynn, and H. L. Davis, Phys. Rev. B **21**, 4118 (1980)

[25] R. J. Birgeneau, H. J. Guggenheim, and G. Shirane, Neutron Scattering Investigation of Phase Transitions and Magnetic Correlations in the Two-Dimensional Antiferromagnets K_2NiF_4, Rb_2MnF_4, Rb_2FeF_4, Phys. Rev. B **1**, 2211 (1970).

[26] X. H. Chen, T. Wu, G. Wu, R. H. Liu, H. Chen, and D. F. Fang, Superconductivity at 43K in $SmFeAsO_{1-x}F_x$, Nature **453**, 761 (2008).

[27] R. König, A. Schindler, and T. Herrmannsdörfer, Superconductivity of Compacted Platinum Powder at Very Low Temperatures, Phys. Rev. Lett. **82**, 4528 (1999).
[28] C. Kittel, *Introduction to Solid State Physics*, 8th ed. (John Wiley and Sons, USA, 2005), Chap. 11, pp. 297-320.
[29] P. Ehrenfest, Physica (The Hague) **5**, 388 (1925).
[30] W. J. De Haas, Diamagnetism, Field Strength, and Crystal Structure, Nature **127**, 335 (1931).
[31] Y. Hasegawa, P. Lederer, T. M. Rice, and P. B. Wiegmann, Theory of Electronic Diamagnetism in Two-Dimensional Lattices, Phys. Rev. Lett. **63**, 907 (1989).
[32] T. Hirose, Y. Okamoto, J.-I Yamaura, and Z. Hiroi, Large Diamagnetic Susceptibility from Petit Fermi Surfaces in LaV_2Al_{20}, J. Phys. Soc. Jpn. **84**, 113701 (2015).